ELSEVIER

Journal of Hydrology 254 (2001) 82–101

Journal of Hydrology

www.elsevier.com/locate/jhydrol

Catchment-scale advection and dispersion as a mechanism for fractal scaling in stream tracer concentrations

James W. Kirchner[a,*], Xiahong Feng[b], Colin Neal[c]

[a]*Department of Earth and Planetary Science, University of California, Berkeley, CA 94720-4767, USA*
[b]*Department of Earth Sciences, Dartmouth College, Hanover, NH 03755, USA*
[c]*Centre for Ecology and Hydrology, McLean Building, Wallingford, Oxon OX 10 8BB, UK*

Received 26 October 2000; revised 8 June 2001; accepted 3 July 2001

Abstract

Time series of chemical tracers in rainfall and streamflow can be used to probe the internal workings of catchments. We have recently proposed that catchments act as fractal filters for inert chemical tracers like chloride, converting 'white noise' rainfall chemistry inputs into fractal '1/*f* noise' chemical time series in runoff [Nature 403 (2000) 524]. This implies that catchments have long-tailed travel-time distributions, and thus retain soluble contaminants for unexpectedly long timespans. Here we show that these long-tailed travel-time distributions, and the fractal tracer time series that they imply, can be generated by advection and dispersion of spatially distributed rainfall inputs as they travel toward a channel. Tracer pulses that land close to the stream reach it promptly, with relatively little dispersion. Tracer pulses that land farther upslope must travel farther to reach the stream, and undergo more dispersion. The tracer signal in the stream will be the integral of the contributions from each point along the length of the hillslope, with a peak at short lag times (reflecting tracers landing near the stream) and a long tail (reflecting tracers landing farther from the stream). Here we integrate the advection–dispersion equation for rainfall tracers landing at all points on a simple model hillslope, and show that it yields fractal tracer behavior, as well as a travel-time distribution nearly equivalent to that found empirically [Nature 403 (2000) 524]. However, it does so only when the dispersion length scale approaches the length of the hillslope, implying that subsurface transport is dominated by large conductivity contrasts related to macropores, fracture networks, and similar large-scale heterogeneities in subsurface conductivity. Thus, the 1/*f* scaling observed at our study sites indicates that these catchments are dominated by flowpaths that exhibit macro-dispersion over the longest possible length scales.

Keywords: Runoff; Ground water; Watershed; Catchment; Contaminant transport; Spectral analysis

1. Introduction

The travel time of water through a catchment — i.e. the time it takes for rainwater to travel to the stream- controls the persistence of soluble contaminants, and thus the downstream consequences of pollution episodes (Langmuir, 1997; Schnoor, 1996). A catchment is characterized by a distribution of travel times, reflecting the diverse flow paths that rainfall can take to the stream. Quantifying this travel-time distribution is essential to predicting the transport and fate of soluble contaminants. Consider, for example, the downstream consequences of a brief contaminant pulse in the rain falling on a catchment. If the catchment transmits most of its rainfall promptly to the stream, then the contaminant pulse in the stream will be brief, but it

* Corresponding author. Tel.: +1-510-643-8559; fax: +1-510-643-9980.
E-mail address: kirchner@seismo.berkeley.edu (J.W. Kirchner).

0022-1694/01/$ - see front matter
PII: S0022-1694(01)00487-5

Table 1
Plynlimon study catchments. Catchment soils are classified as moorland (M), podzol (P) or gley (G); vegetation cover is classified as moorland (M) or Sitka Spruce (SS)

Site	Drainage area (km^2)	Soils	Vegetation	Felling history	Records analyzed
Hafren	3.47	M/P/G	M/SS	Ongoing thinning	Weekly 1983–97, daily 1994–97
Tanllwyth	0.51	G	SS	50%, 1996	Weekly 1991–97, daily 1994–97
Hore	3.35	M/P/G	SS	50%, 1985–88	Weekly 1983–97
Upper Hore	1.78	M/P/G	SS	None	Weekly 1985–97
South2 Hore	0.05	P	SS	100%, 1989	Weekly 1988–97

will also be intense. Conversely, if the catchment's distribution of travel times is broad — for example, if rainfall inputs are extensively mixed with large volumes of pre-storm water stored in the subsurface — then the contaminant flux that reaches the stream will be much less intense, but it will also be much more persistent. These two styles of contaminant delivery may have very different ecological consequences, depending on the characteristics of the contaminant in question.

A catchment's travel-time distribution is intimately connected to its dominant flowpaths (McDonnell et al., 1991). Thus, the travel-time distributions that characterize catchments should help to clarify the mechanisms that control flow routing in the subsurface. (Travel times through the channel network are typically much faster than through the subsurface, so channel network geometry should exert only second-order control on the travel-time distribution.) The timescales of transport and storage in catchments are also important for predicting the extent to which rainfall inputs will be chemically modified by reactions with catchment soils and bedrock (Burns et al., 1998). However, despite the obvious importance of catchment travel-time distributions for watershed hydrology and geochemistry, they have rarely been quantified. Tracer breakthrough curves have been used to estimate travel times between specific tracer injection points and catchment outlets (e.g. Nyberg et al., 1999), and in at least one case, a travel-time distribution has been estimated for a small experimental catchment by manipulating the isotopic signature of its entire precipitation input (Rodhe et al., 1996). Natural fluctuations in chemical and isotopic tracers have been widely used to estimate the 'new water' and 'old water' contributions in individual storm events (e.g. Kendall et al., 1995; McDonnell et al., 1991; Neal and Rosier, 1990; Sklash, 1990). However, their potential for measuring catchment travel times over longer timescales remains largely unexplored (but for an exception, see Soulsby et al., 2000).

We have recently used natural fluctuations of chloride concentrations in rainfall and streamflow to estimate the travel-time distribution for the Hafren catchment at Plynlimon, Wales (Kirchner et al., 2000). Our analysis showed that chloride fluctuations in streamflow were strongly damped relative to those in rainfall, on all but the longest timescales, implying that the catchment retains a long chemical memory of the inert chloride tracer. The Hafren catchment acts as a fractal filter, in which rainfall chloride fluctuations with an approximate 'white noise' power spectrum are converted into streamflow chloride fluctuations with a fractal '1/*f* noise' spectrum. In 1/*f* noise, the spectral power of fluctuations (i.e. the square of their amplitude) is inversely proportional to their frequency — or, equivalently, is proportional to their wavelength. Time series characterized by 1/*f* scaling therefore lack a characteristic timescale, because fluctuations at any wavelength are embedded in larger-amplitude fluctuations at longer wavelengths, and these, in turn, are embedded in still larger fluctuations on still longer timescales. Chloride fluctuations in Hafren streamflow exhibit fractal 1/*f* scaling over three orders of magnitude. This implies that the travel-time distribution for the Hafren catchment is an approximate power law, scaling as $\tau^{-0.5}$ for travel times τ that are short compared to the mean travel time τ_0.

Here, we extend our earlier analysis in two ways. First, we show that the fractal scaling observed at the Hafren catchment also characterizes four other

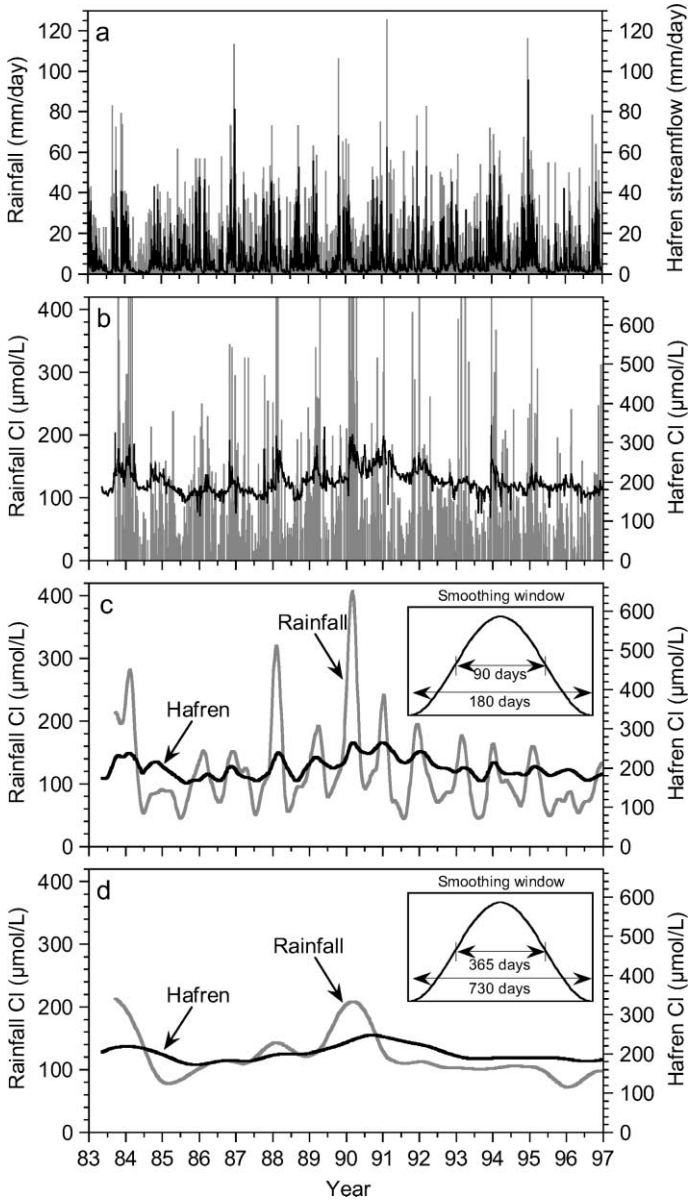

Fig. 1. Time series of daily water fluxes and weekly chloride concentrations in rainfall (gray lines) and Hafren streamflow (black lines) at Plynlimon, mid-Wales. Streamflow response to rainfall inputs is prompt, with little attenuation (a), whereas weekly fluctuations in streamflow concentrations are damped significantly compared to rainfall (b). Seasonal fluctuations in rainfall concentrations vary greatly from year to year; seasonal fluctuations in streamflow concentrations are much smaller (c). Even inter-annual fluctuations in streamflow concentrations are damped compared to those in rainfall (d). The streamflow concentration scale has been expanded by a factor of 1.60, to account for dry deposition and evapoconcentration; i.e. the weighted average concentrations of chloride in rainfall and streamflow would overlap exactly on the graphs.

sampling sites at Plynlimon, suggesting that it may be a general property of many different types of catchments. Second, we show that this fractal scaling can arise from the advection and dispersion of rainfall inputs distributed across a catchment, as they travel downslope toward the stream.

2. Fractal tracer fluctuation scaling and power-law travel-time distributions at Plynlimon

Catchments are spatially complex and subsurface flow is invisible, so transport and mixing in catchments can only be observed indirectly, using isotopic and chemical tracers (e.g. Soulsby et al., 2000). Chloride is an effective chemical tracer (Neal and Rosier, 1990), because it is nonreactive under typical catchment conditions; ^{18}O or deuterium could also be used as tracers, but long-term high-resolution time series of these isotopes are rare. We analyzed chloride concentrations in rainfall and streamflow at five small ($0.05–3.5\ km^2$) catchments at Plynlimon, Wales (Table 1); the catchments and the data sets are described in detail elsewhere (Neal and Kirchner, 2000; Neal et al., 1997a). Plynlimon is close to the Welsh coastline, and seasalt chloride inputs fluctuate greatly from one storm to the next, reflecting variations in storm trajectories. By comparing the chloride signatures of rainfall and runoff through time, we can measure how long the catchments retain a chemical memory of the rain that has fallen on them (Neal et al., 1988; Robson et al., 1993).

At Plynlimon, storm rainfall inputs are usually matched by prompt (and roughly equal) changes in streamflow (Fig. 1a), whereas streamflow chloride concentrations exhibit strongly damped response to rainfall chloride inputs (Fig. 1b). This indicates that peak flows consist mostly of pre-storm water released from the catchment, rather than rainfall flowing directly into the stream (Neal et al., 1988). Thus, the timescales of hydrologic and chemical response are decoupled, with chemically 'old' water being released promptly in response to 'new water' inputs (Buttle, 1994; Sklash et al., 1996). But how old is this old water? The water reaching the stream at any given time will be a mixture of rainfall that has fallen on each point in the catchment at various times in the past, weighted by the travel-time distributions that characterize the flowpaths connecting each point with the stream. Obviously, the intricate spatial complexity of real-world catchments makes it impossible to map these flowpaths in detail. However, it may nonetheless be possible to describe their aggregate effects with simple conceptual models that can be tested against catchment-scale input and output time series. The purpose of this paper is to illustrate this approach.

One can begin to probe the chemical 'memory' of the Plynlimon catchments by comparing their tracer concentrations in rainfall and streamflow, averaged over different spans of time. For example, seasonal fluctuations in rainfall chloride concentrations are large and highly variable from year to year, whereas seasonal fluctuations in streamflow chloride are much smaller (Fig. 1c). This indicates that the streamflow chloride signal averages together inputs from high-chloride and low-chloride seasons, and thus implies that the catchments retain significant volumes of water from one season to the next. Even annually averaged chloride concentrations are more variable in rainfall than in streamflow (Fig. 1d), indicating that the catchments are storing and mixing enough water to affect runoff chloride concentrations from one year to the next. Note that high-chloride seasons, such as the winters of 1984 and 1990, elevate streamflow chloride concentrations for several years, indicating that the catchments must be retaining significant volumes of water on long timescales.

This intuitive approach can be made more precise using spectral analysis, which decomposes the rainfall and streamflow signals into their component wavelengths (Bracewell, 2000; Scargle, 1982), and measures the spectral power (the square of the amplitude) at each wavelength. The relationship between the spectral power of the input (rainfall) and output (streamflow) at each wavelength reflects how strongly the catchment attenuates hydrologic and chemical signals on each timescale. The power spectra of streamflow water fluxes at Plynlimon nearly equal the rainfall power spectrum (Fig. 2a), indicating that the catchments transmit hydrologic signals with little damping, on all but the shortest timescales. The power spectra of streamflow chloride, by contrast, are strongly attenuated compared to rainfall on all wavelengths shorter than several years, with progressively greater attenuation at shorter wavelengths (Fig. 2b–f).

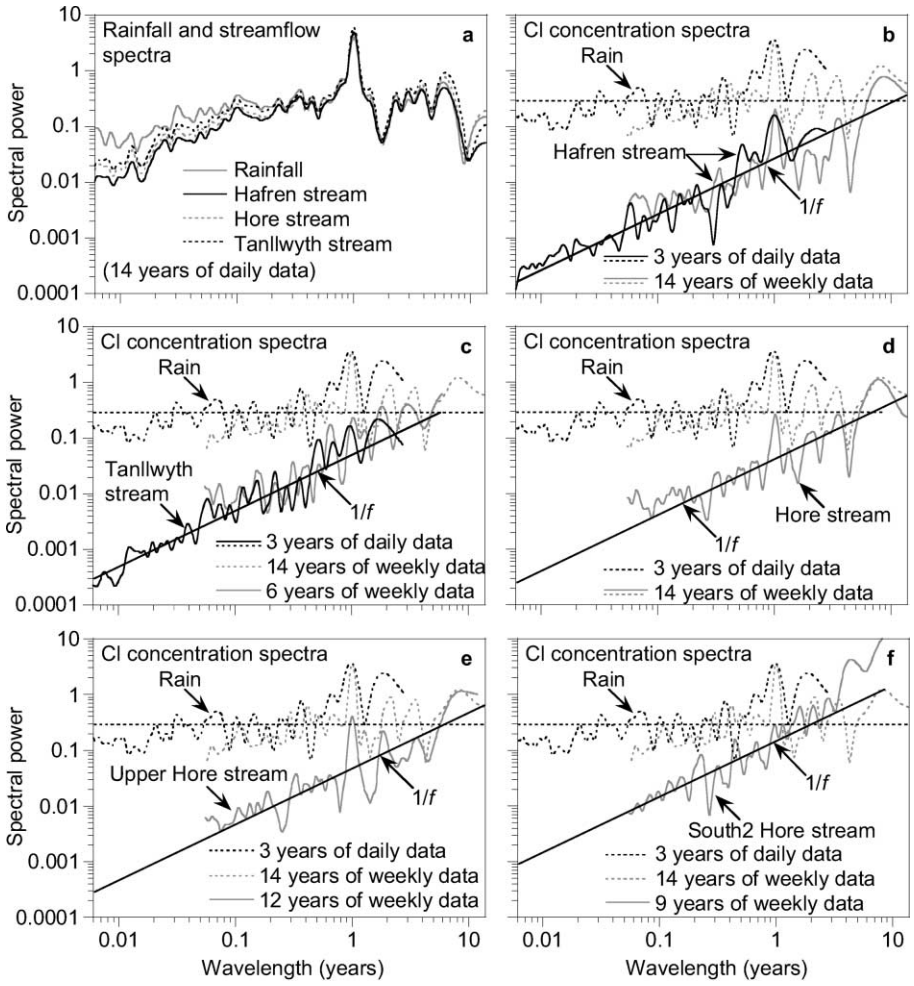

Fig. 2. Power spectra of water fluxes and chloride concentrations at Plynlimon, Wales. The water flux spectra (a) indicate little damping, except at the shortest timescales, whereas the chloride concentration spectra (b–f) show strong attenuation, except at the longest timescales. The chloride spectra of rainfall (dotted lines) resemble white noise (and are the same in each panel); those of streamflow (solid lines) resemble 1/*f* noise, with spectral power increasing proportionally to wavelength across the entire range of scales. For ease of interpretation, the spectra are shown as functions of wavelength (1/frequency) rather than frequency. Panels (c)–(f) show chloride concentration spectra for four other sampling sites at Plynlimon. Daily chloride concentration data (solid black lines) are available only for Hafren (b) and Tanllwyth (c); weekly stream concentrations (solid gray lines) are available, for varying timespans, at every site. Upper Hore (e) is a sampling point halfway up the Hore catchment (d); below this point most of the Hore catchment was clearfelled during the first half of the period of record. South2 Hore (f) is a small hillslope tributary in the clearfelled zone. Its unusually high spectral power at long wavelengths is caused by non-stationarity in its time series, which may be associated with clearfelling during the second year of its nine-year sampling record. Because the rainfall chloride time series have gaps (since rainfall concentrations are undefined on dates without rain), we used the Lomb–Scargle Fourier transform, which has the same statistical properties as the conventional Fast Fourier Transform, but does not require evenly spaced data (Scargle, 1982).

Except for a strong annual peak and its subharmonics (which reflect seasonal fluctuations), the rainfall chloride spectrum scales roughly as white noise. The streamflow chloride spectra, by contrast, show fractal power-law scaling that resembles 1/*f* noise (Fig. 2b–f); this indicates that these catchments are acting as fractal filters, converting white noise inputs into 1/*f* noise outputs spanning three orders of magnitude (i.e. over timescales of days to several years).

This scaling behavior is directly related to the

catchments' travel-time distributions. If a catchment's travel-time distribution is broad compared to the wavelength of a chloride fluctuation in the rainfall, waters from high-chloride and low-chloride rainfall inputs in the past will be mixed together in the stream. This mixing implies that the chloride fluctuations will be averaged together, and thus will be damped. The shorter the wavelength of the chloride fluctuation in rainfall compared to the catchment's travel-time distribution, the greater the number of high-chloride and low-chloride fluctuations that are averaged together, and the stronger this attenuation by averaging becomes. Conversely, chloride variations on timescales that are long compared to the travel-time distribution will be transmitted through the catchment without significant attenuation.

The relationship between a catchment's travel-time distribution and its power spectrum can be made mathematically explicit (Duffy and Gelhar, 1985, 1986). The travel-time distribution determines how much of today's rainfall will reach the stream tomorrow, the day after tomorrow, and so forth. Thus, the present concentration of a conservative tracer in the stream will reflect the rainfall concentrations throughout the past, weighted by their fractional contribution to the present runoff. In other words, the stream concentration $c_S(t)$ at any time t is the convolution of the travel-time distribution $h(\tau)$ and the rainfall concentrations $c_R(t-\tau)$ throughout the past, where τ is the lag time between rainfall and runoff:

$$c_S(t) = \int_0^\infty h(\tau) c_R(t-\tau)\, d\tau \tag{1}$$

Because the flow rate varies through time, Eq. (1) is strictly valid when t and τ are expressed in terms of the cumulative flow through the catchment, rather than calendar time (Niemi, 1977; Rodhe et al., 1996), but the mathematics are the same in either case (Niemi, 1977). We analyzed the Plynlimon data both ways and obtained functionally equivalent results, so for simplicity we use the time-based formalism here. Eq. (1) implies that

$$C_S(f) = H(f) C_R(f) \qquad \text{and}$$
$$|C_S(f)|^2 = |H(f)|^2 |C_R(f)|^2 \tag{2}$$

where f is frequency (cycles/time); $C_S(f)$, $H(f)$, and $C_R(f)$ are the Fourier transforms of $c_S(t)$, $h(\tau)$, and $c_R(t-\tau)$; and $|C_S(f)|^2$, $|H(f)|^2$, and $|C_R(f)|^2$ are their power spectra (Gelhar, 1993). In our case, because the rainfall concentration spectrum is nearly white noise ($|C_R(f)|^2 \approx$ constant), the spectrum of the travel-time distribution is roughly proportional to the runoff concentration spectrum ($|H(f)|^2 \propto |C_S(f)|^2$).

In our earlier work, we demonstrated that the scaling behavior shown in Fig. 2b–f is inconsistent with two commonly used conceptual models for catchments. Catchments are often modeled as well-mixed reservoirs, implying that their travel-time distributions should be exponentials with the characteristic form

$$h(\tau) = \frac{1}{\tau_0} e^{-\tau/\tau_0} \qquad \text{or} \qquad h(\tau/\tau_0) = e^{-\tau/\tau_0} \tag{3}$$

where τ is the travel time, and τ_0 is the mean travel time (or, equivalently, the volume of water stored in the catchment divided by the average flow rate). Eq. (3) implies a power spectrum of the form

$$|H(f)|^2 = (1 + 4\pi^2 f^2 \tau_0^2)^{-1} \qquad \text{or}$$
$$|H(\lambda)|^2 = \frac{\lambda^2}{(\lambda^2 + 4\pi^2 \tau_0^2)} \tag{4}$$

where λ is wavelength ($f = 1/\lambda$). Eq. (4) has a power-law slope of 2 for wavelengths of $\lambda \ll 2\pi\tau_0$, inconsistent with the power spectra in Fig. 2b–f, which have a power-law slope near 1. Alternatively, catchments are sometimes modeled by advection and dispersion along a flowpath of fixed length, but this yields no power-law scaling at all (Kirchner et al., 2000), which is clearly inconsistent with the power spectra in Fig. 2.

The fractal $1/f$ scaling shown in Fig. 2b–f is, however, consistent with a gamma distribution of travel times

$$h(\tau) = \frac{\tau^{\alpha-1}}{\beta^\alpha \Gamma(\alpha)} e^{-\tau/\beta} \tag{5}$$

where α is a shape parameter and $\beta = \tau_0/\alpha$ is a scale parameter. When $\alpha = 0.5$, the gamma distribution becomes

$$h(\tau/\tau_0) = \sqrt{\frac{1}{2\pi(\tau/\tau_0)}} e^{-(1/2)\tau/\tau_0} \tag{6}$$

where a factor of τ_0, the average travel time, has been

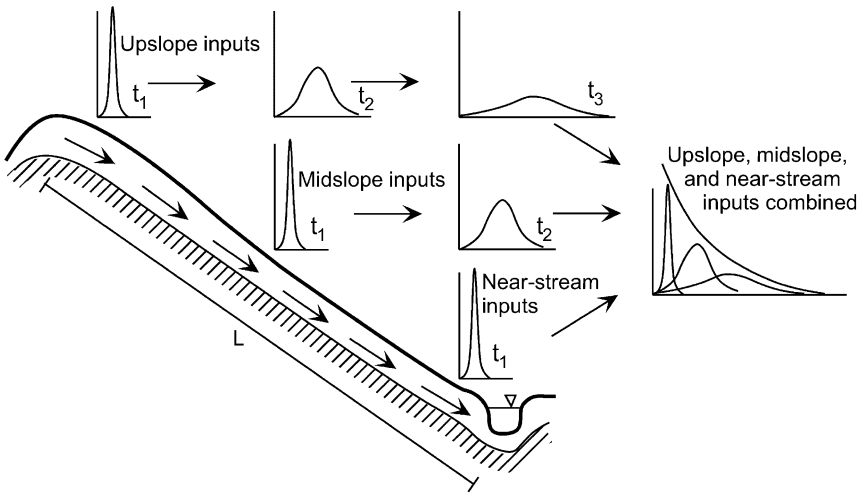

Fig. 3. Conceptual model of dispersion of spatially distributed tracer inputs, as they advect down a hillslope cross-section en route to a stream channel. Tracer pulses that land close to the stream reach it promptly, with relatively little dispersion. Tracer pulses that land farther upslope must travel farther to reach the stream, and undergo more dispersion. The tracer signal in the stream will integrate the contributions from each point along the length of the hillslope, with a peak at short lag times (reflecting tracers landing near the stream) and a long tail (reflecting tracers landing farther upslope).

introduced by the change of variables in re-casting $h(\tau)$ as $h(\tau/\tau_0)$. In contrast to the conventional models described above, the gamma distribution can simultaneously exhibit both long-term memory of past inputs (because it has a broad tail, proportional to $\tau^{-0.5}$, before falling off as $e^{-\tau/2\tau_0}$ in the limit of large τ), and short-term responsiveness to rainfall inputs (because $\tau^{-0.5}$ rises toward infinity as τ approaches zero, but does so in such a way that its integral is finite). With $\alpha = 0.5$, the gamma distribution's power spectrum (Bain, 1983)

$$|H(f)|^2 = (1 + 16\pi^2 f^2 \tau_0^2)^{-1/2} \quad \text{or}$$

$$|H(\lambda)|^2 = \frac{\lambda}{\sqrt{\lambda^2 + 16\pi^2 \tau_0^2}} \tag{7}$$

agrees well with the observed power spectra (Fig. 2b–f), with a power-law slope of 1 for $\lambda \ll 4\pi\tau_0$.

Thus, the gamma distribution is an empirically adequate description of the scaling behavior seen at the Plynlimon catchments. However, the mechanistic basis for this travel-time distribution, and thus for the fractal scaling behavior that it implies, has until now remained unclear. We have previously suggested that the fractal scaling behavior observed at Plynlimon might reflect the fractal characteristics of soil pores and bedrock fractures, or that, alternatively, it may arise through more prosaic mechanisms, such as advection and dispersion along an ensemble of flowpaths connecting the stream with the surrounding catchment area (Kirchner et al., 2000). Here, we explore a simple model for advection and dispersion of spatially distributed rainfall inputs. We show that with plausible parameter values, this simple conceptual model yields travel-time distributions similar to Eq. (6), and power spectra like those observed at Plynlimon.

3. A conceptual model of advection and dispersion of spatially distributed inputs in catchments

In small upland catchments like Plynlimon, the great majority of runoff reaches the stream by flowing downslope in the shallow subsurface, either through the soil matrix, along the soil/bedrock contact, or within the upper few meters of fractured bedrock (e.g. Anderson and Burt, 1990; Anderson et al., 1997; Bishop et al., 1990; Dunne, 1978; Montgomery et al., 1997; Soulsby et al., 1998). Because most of the downslope flow occurs in a layer just a few meters

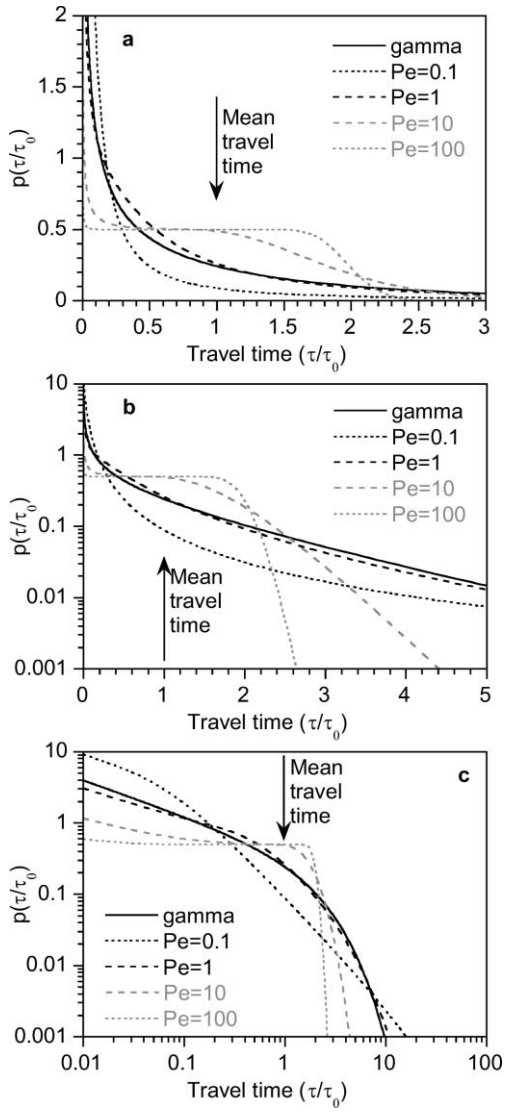

Fig. 4. Catchment travel-time distributions predicted by the spatially distributed advection–dispersion model (Eq. (11)) for a range of Peclet numbers, compared to the empirical gamma distribution (Eq. (6)). The advection–dispersion model strongly resembles the gamma distribution for Peclet numbers near 1, but diverges from it for $Pe \gg 1$ and $Pe \ll 1$. The same curves are shown on three different sets of coordinate axes (linear, semi-log, and double-log), in order to illustrate their general shape (a), as well as their upper and lower tails (b,c).

thick — whereas hillslope lengths are typically 100s of meters — the flow down a hillslope cross-section (e.g. Fig. 3) is very nearly one-dimensional. Here, therefore, we develop a one-dimensional model of advection and dispersion along a hillslope cross-section (Fig. 3), in which water flows downhill through a shallow subsurface layer (here, 'shallow' means that the thickness of the subsurface flowing layer is much less than its length L). Let us assume for simplicity that bulk advection through this layer occurs at a fixed velocity, determined by the hydraulic conductivity and the slope of the underlying impermeable layer. As a thought experiment, assume a steady rainfall rate, introduce a brief tracer pulse into the rainfall, and then consider how the tracer pulse will advect and disperse downslope (Fig. 3). Tracer pulses that land close to the stream will reach it quickly, and will undergo relatively little dispersion. Tracer pulses that land farther upslope must travel farther to reach the stream, and will undergo more dispersion, so the signals that they add to the stream will be more spread out in time. The tracer signal in the stream will be the integral of the contributions from each point along the length of the hillslope, with a peak at short lag times (reflecting tracers landing near the stream) and a long tail (reflecting tracers landing farther from the stream).

We can make this intuitive picture more mathematically explicit. A tracer pulse that lands a distance x from the stream, advects downslope at a velocity v, and undergoes dispersion at a rate determined by the dispersion coefficient D, will arrive at the stream with a distribution of travel times determined by the solution to the advection–dispersion equation (Kreft and Zuber, 1978):

$$p(x,\tau) = \frac{x}{\sqrt{4\pi D\tau^3}} \mathrm{e}^{-(x-v\tau)^2/(4D\tau)} \tag{8}$$

It is the fact that inputs enter the system along its entire length that distinguishes the model in Fig. 3 from the fixed-length advection–dispersion model, which we have previously shown is inconsistent with the scaling behavior observed at Plynlimon. To determine the travel-time distribution of tracers arriving at the stream, we need to average Eq. (8) from the streambank ($x = 0$) to the hilltop ($x = L$)

$$h(\tau) = \frac{\int_{x=0}^{L} p(x,\tau)w(x)\,\mathrm{d}x}{\int_{x=0}^{L} w(x)\,\mathrm{d}x} \tag{9}$$

where $w(x)$ is a weighting function that is proportional

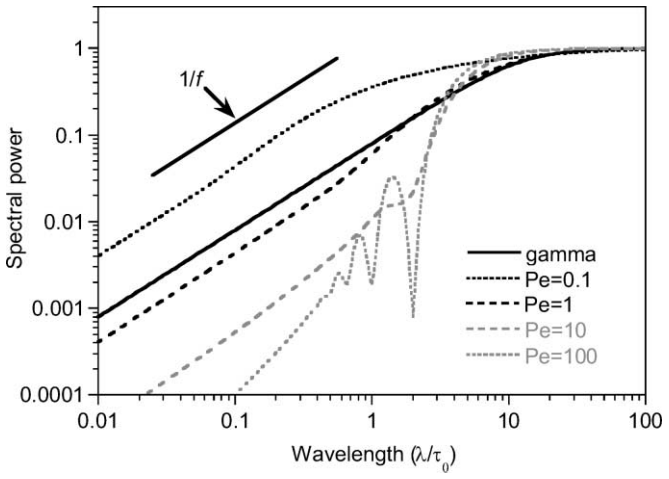

Fig. 5. Power spectra of the spatially distributed advection–dispersion model, compared to the power spectrum of the empirical gamma distribution (Eq. (7)) and the 1/*f* scaling observed in the Plynlimon data. The advection–dispersion model's power spectrum resembles the gamma distribution's spectrum for Peclet numbers near 1, and exhibits 1/*f* scaling for a range of Peclet numbers around 1.

to the fraction of the catchment's surface area at any distance x from the stream (thus accounting for the shape of the catchment). For the one-dimensional model shown in Fig. 3, $w(x)$ is a constant and Eq. (9) can be solved analytically, yielding

$$h(\tau) = \frac{1}{L}\sqrt{\frac{D}{\pi\tau}}\left[e^{-(-v\tau)^2/4D\tau} - e^{-(L-v\tau)^2/4D\tau}\right] + \frac{v}{2L}\left[\mathrm{erf}\left(\frac{L-v\tau}{\sqrt{4D\tau}}\right) - \mathrm{erf}\left(\frac{-v\tau}{\sqrt{4D\tau}}\right)\right] \quad (10)$$

One can see that in the limit as τ approaches zero, the travel-time distribution shown in Eq. (10) is roughly proportional to $\tau^{-0.5}$, just like the gamma distribution shown in Eq. (6). Equation (10) appears to depend on three separate parameters: the hillslope length L, the advective velocity v, and the diffusion constant D. However, it can be simplified to a single-parameter model by two transformations of variables. First, we non-dimensionalize the rate of dispersion using the average Peclet number $Pe = vL/2D$, i.e. the ratio of the timescales of advective and dispersive transport from the middle of the hillslope. Second, we re-express the travel time τ as a dimensionless ratio with the average travel time $\tau_0 = L/2v$, i.e. the time required for advective transport from the middle of the hillslope to the stream. With these substitutions, Eq. (10) becomes a function only of the Peclet number and the dimensionless travel time τ/τ_0

$$h(\tau/\tau_0) = \underline{\underline{\sqrt{\frac{1}{4\pi Pe(\tau/\tau_0)}}e^{-1/4Pe(\tau/\tau_0)}[1 - e^{(z_0)^2-(z_L)^2}]}} + \frac{1}{4}[\mathrm{erf}(z_L) - \mathrm{erf}(z_0)] \quad (11)$$

where

$$z_0 = -\frac{1}{2}\sqrt{Pe\tau/\tau_0} \quad \text{and} \quad z_L = \sqrt{Pe/(\tau/\tau_0)} - \frac{1}{2}\sqrt{Pe\tau/\tau_0} \quad (12)$$

The double-underlined terms in Eq. (11) have the same general form as the gamma distribution given in Eq. (6). As Fig. 4 shows, Eq. (11) is a good approximation of the gamma distribution when the Peclet number is near 1, i.e. when advection and dispersion are of roughly equal effectiveness in transporting the tracer to the stream. Thus, our simple advection–dispersion system with spatially distributed inputs (Fig. 3) can yield an approximate gamma distribution of travel times, but only when dispersion is a significant component of the solute flux.

Since the primary evidence for a gamma-like

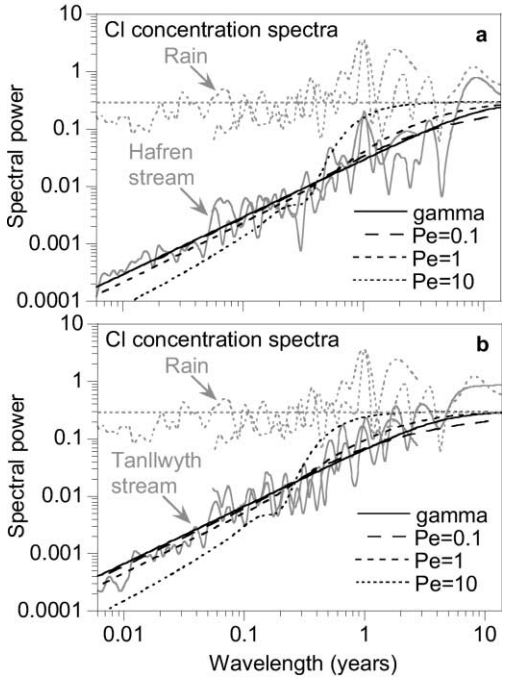

Fig. 6. Best-fit power spectra of the advection–dispersion model (Eq. (11)) and the gamma distribution (Eq. (6)), fitted to the Plynlimon data by adjusting the mean travel time τ_0. At Peclet numbers near 1 or less, the advection–dispersion model fits the observed chloride spectra at least as well as the gamma distribution does. At Peclet numbers near 10 or higher, the advection–dispersion model's power spectrum is inconsistent with the Plynlimon data.

distribution of travel times is the $1/f$ scaling we have observed in streamflow chloride concentrations, it is important to determine whether the spectral properties of the spatially distributed advection–dispersion model (Eq. (11)) are consistent with the fractal filtering behavior shown in Fig. 2 above. The power spectrum of the travel-time distribution can be estimated by taking the Fourier transform, by numerically integrating

$$H(f) = \int h(\tau)\, e^{-i2\pi f\tau}\, d\tau \tag{13}$$

The spectral power is then calculated by multiplying the Fourier transform $H(f)$ by its complex conjugate. As Fig. 5 shows, the power spectrum of the spatially distributed advection–dispersion model exhibits $1/f$ scaling at wavelengths λ shorter than the mean travel time τ_0, for a range of Peclet numbers near 1. At Peclet numbers much greater than 1, the model deviates substantially from $1/f$ scaling.

We can fit the power spectra of the travel-time distributions to the observed streamflow chloride spectra by adjusting the mean travel time τ_0. As Fig. 6 shows, the spatially distributed advection–dispersion model almost exactly matches the gamma distribution (and thus fits the streamflow spectra as well as the gamma model does) for Peclet numbers in the range of 0.1–1. However, power spectra for Peclet numbers on the order of 10 or greater are inconsistent with the observed power spectra at Plynlimon.

The best-fit travel times τ_0 are roughly half as long at Tanllwyth as at Hafren, for both the advection–dispersion and gamma models (Table 2). The Hafren catchment is dominated by podzolic soils, which are more permeable than the gleys that dominate the Tanllwyth catchment. Thus, one would expect that the Tanllwyth catchment should have less capacity to store water, and greater potential for rapid near-surface runoff. This expectation is consistent with the shorter mean residence time τ_0 implied by the Tanllwyth power spectra.

Table 2
Mean travel times and dispersivities implied by best-fit power spectra

		Mean travel time (yr)	
Model	Dispersivity (α_L)	Hafren	Tanllwyth
Gamma distribution (Eq. (6))	n/a	0.82 ± 0.02	0.36 ± 0.01
Spatially distributed advection and dispersion (Eq. (11))			
$Pe = 0.1$	$5L$	4.32 ± 0.11	1.98 ± 0.05
$Pe = 1$	$0.5L$	0.58 ± 0.01	0.28 ± 0.01
$Pe = 10$	$0.05L$	0.18 ± 0.01	0.11 ± 0.01

4. Discussion

Our analysis has shown that downslope advection and dispersion of spatially distributed rainfall inputs should cause fractal filtering of their tracer concentrations, similar to that observed in the chloride tracer time series at Plynlimon. We have thus shown that, as an explanation for the fractal scaling in the Plynlimon data, catchment-scale advection and dispersion is a phenomenologically adequate hypothesis. But is it a mechanistically plausible one? For the hypothesis to be mechanistically plausible, at least two conditions must be met. First, its premises must be reasonable, at least as an approximation to the intricate complexity of real-world catchments. Second, its parameter values, when fitted to the data, must be realistic. We consider each of these issues in turn.

Our analysis is based on a highly idealized catchment cross-section, in which downslope flow is confined to a thin conducting layer (e.g. at the interface between highly permeable soils and highly impermeable bedrock). The Plynlimon catchments, by contrast, are underlain by deeply fractured shales, slates, and grits, with flow occurring at a range of depths. Neal et al. (1997b) detected groundwater at each of 13 boreholes drilled in the Hafren catchment. Ten of these boreholes were shallow (<15 m depth), and groundwater levels were typically less than 10 m below the surface; inputs to the boreholes were localized as fracture flows and water levels fluctuated by as much as 3 m. In three deeper boreholes (up to 50 m depth), groundwater was encountered at a range of depths; water level and water quality fluctuations in these boreholes implied more rapid circulation and greater storage at depths of less than 10 m. There is also strong evidence that these shallower groundwaters are in hydraulic contact with the soils and, in places, in direct contact with the stream (Neal et al., 1997c). Studies now underway using nested sequences of shallow boreholes along hillslope transects at Plynlimon show stratification, with an extremely hydrologically active shallow (<10 m) fracture flow system (A. Haria and P. Shand, personal communication). Considered together, these lines of evidence indicate that the bulk of subsurface transport at Plynlimon takes place at depths that are small compared to the typical hillslope length (100s of meters). Thus, the cross-sectional geometry depicted in Fig. 3 seems reasonable to us as a rough approximation.

Our analysis also assumes a simple planform geometry, characterized by a constant increment of contributing area at any distance x from the channel. We explore the effects of catchment planform geometry on travel-time distributions and power spectra in Appendix A; that analysis demonstrates that the only catchment geometry that fails to produce fractal $1/f$ scaling is one in which the entire catchment runoff converges to a single channel head, with no lateral stream inputs. In that end-member case, the near-stream inputs that are responsible for the catchment's short-term response (see Fig. 3) are outweighed by highly dispersed inputs from upslope. The Plynlimon catchments do not resemble this end-member case, instead having stream channels that extend a significant fraction of the catchments' lengths. Within the range of geometries present at Plynlimon, the spatially distributed advection–dispersion model yields fractal $1/f$ scaling, similar to that seen in the time series data (see Appendix A).

The third major premise of our analysis is that water advects downslope at a constant speed. In reality, we would expect the bulk advection speed to be highly variable, both spatially and temporally. The spatial variations in advection speed (which arise primarily from heterogeneities in hydraulic conductivity) are, of course, a major mechanism underlying macro-dispersion at catchment scale. In this sense, spatial variations in advective transport underlie our analysis, although they are represented in the equations implicitly rather than explicitly. Temporal fluctuations in advection speed can be accommodated by re-casting the time variable in terms of cumulative flow through the catchment rather than cumulative time on a clock (Niemi, 1977; Rodhe et al., 1996). The end result of this approach is a travel-time equation of exactly the same form as Eqs. (11) and (12), but with τ replaced everywhere by Q, the cumulative flow through the catchment, and τ_0 replaced everywhere by Q_0, the volume of water stored in the catchment (this implicitly assumes that diffusion is a trivial component of total dispersion, which is reasonable for near-surface flow like that considered here). Because the travel-time equation is the same, it yields $1/f$ scaling just like the analysis presented above, but with wavelengths measured in units of flow rather than

units of time. The Plynlimon catchment time series exhibit $1/f$ scaling as a function of cumulative flow as well as elapsed time, so the model predictions and the observed data resemble one another in the flow domain as well as the time domain.

The fourth, and most fundamental, premise of our analysis is that solute transport occurs by advection and dispersion, of a kind that is adequately captured by Eq. (8). One check on this premise is to ask whether the parameter values implied by the fits to the data (Fig. 6) are realistic. Reviews by Neuman (1990) and Gelhar et al. (1992) show that field measurements of advective–dispersive transport over distances of 100s of meters (comparable to the flow distances in our catchments) typically yield Peclet numbers on the order of 10, with a few values as low as 1 or as high as 100 or more. Fig. 6 implies that if transport at Plynlimon is governed by classical advection and dispersion, its average Peclet number must be on the order of 1, at the low end of the range observed elsewhere, since Peclet numbers of 10 or 100 are inconsistent with the Plynlimon data.

A further constraint is provided by the average travel times τ_0 that are needed to fit the advection–dispersion model to the Plynlimon data. As Table 2 shows, Peclet numbers much less than 1 require unrealistically long mean travel times, on the order of several years. Given annual runoff of roughly 200 cm/yr at Plynlimon (Neal and Kirchner, 2000), a mean travel time of 2–5 yr would imply catchment storage of 400–1000 cm of water in the subsurface, and it is difficult to imagine how this could be accommodated. Thus, for Peclet numbers much less than 1, the spatially distributed advection–dispersion model requires implausibly long travel times, and for Peclet numbers much greater than 1, it predicts power spectra that are a poor match for the scaling behavior that is observed (Fig. 6). These considerations thus constrain the effective Peclet number to $Pe \approx 1$ at Plynlimon, near the low end of the range of values observed elsewhere.

As diffusion is a trivial component of total dispersion, the dispersion coefficient D in Eqs. (8)–(10) can be re-expressed as the product of the advection velocity v and a longitudinal dispersivity length scale α_L, which has units of length. The Peclet number can likewise be re-expressed as the ratio of the catchment length scale (which we have here defined as the average travel distance, $L/2$) to the dispersivity length scale α_L. Thus the Peclet numbers on the order of 1, which can be seen from Fig. 6 to provide a good fit to the time series data, imply dispersivity length scales $\alpha_L = L/(2Pe)$ on the order of the average travel distance (see Table 2). In order for the Plynlimon catchments' fractal filtering behavior to arise from advection and dispersion of spatially distributed rainfall inputs, their characteristic dispersivities must approach the hillslope length.

In summary, an advection–dispersion mechanism like that hypothesized here is consistent with the Plynlimon data, but only with dispersivities of roughly the same scale as the hillslope length itself. These large dispersivities (or, equivalently, small Peclet numbers) are characteristic of a subsurface flow system in which hydraulic conductivity is spatially heterogeneous at all scales, up to the scale of the entire hillslope. Several lines of field evidence support this conceptual picture at Plynlimon. First, fracture-flow-dominated groundwaters have been found at every borehole drilled in the Hafren catchment, whether close to the divide, at mid-slope, or close to the stream (Neal et al., 1997b), implying an extensive fracture system. Second, the chemistry and hydrology of these groundwaters are spatially and temporally variable, implying that the groundwater system is dynamic both physically and chemically across the catchment. Third, flow routing through macropores has been directly observed at Plynlimon, with hydrologic events producing marked, but highly variable, changes in macropore flow, chemistry, and isotopic composition (Chapman et al., 1997; Gilman and Newson, 1980; Muscutt, 1990; Sklash et al., 1996). Finally, runoff in small streams across the Hafren catchment is highly variable both spatially and temporally, exhibiting no consistent correlation with bedrock geology, soil types, geomorphic setting, or location within the catchment, suggesting great variability in what would be termed 'soilwater' and 'ground water' inputs (Hill and Neal, 1997; Neal et al., 1997d).

Thus, the field evidence from Plynlimon indicates a spatially heterogeneous flow system dominated by large conductivity contrasts, consistent with the macro-dispersive flow implied by our analysis. This macro-dispersive behavior implies that the shallow subsurface flow layer must contain a tangle of different flowpaths with widely varying conductivities.

These flowpaths may be distributed laterally across the hillslope (i.e. perpendicular to the plane of Fig. 3), such that solutes that fall equal distances from the stream — but at different locations across the slope — will run off at different speeds. In addition, the conductivity of the shallow groundwater flow system probably decreases with depth; as a result, groundwater flows that are nearer to the surface should transport their solutes more rapidly downslope, creating a macroscopic form of shear dispersion in the subsurface. The exact configuration of flowpaths in the subsurface is not known, nor is it likely to ever be knowable. Thus the challenge of catchment modeling is to introduce as much physical realism as possible, without imposing undue literalism concerning details that are unobservable. The most that can be said at this point is that the fractal chloride tracer spectra imply macro-dispersion at hillslope scale, and thus imply a highly heterogeneous network of fast and slow flowpaths.

It is perhaps surprising that such a prosaic mechanism as advective–dispersive transport could convert non-fractal catchment inputs into fractal outputs. However, while our analysis shows that this simple mechanism could be responsible for the fractal scaling observed at Plynlimon, we emphasize that we have not yet tested several other candidate hypotheses, including mobile–immobile models (e.g. Sposito et al., 1986), fracture flow models (e.g. Dershowitz and Miller, 1995; Tsang and Neretnieks, 1998), two-dimensional flow net models (e.g. Toth, 1963), and transmissivity feedback models (e.g. Bishop, 1991), any or all of which could potentially yield similar fractal scaling. Thus, we cannot yet say whether the fractal scaling in the Plynlimon data is diagnostic of a single generating mechanism.

Our analysis implies that understanding timescales of catchment response may require explicitly acknowledging that catchments are spatially extensive, and that they receive spatially distributed inputs. To our knowledge, no parsimonious zero-dimensional model (such as a simple system of linked 'boxes') can reproduce the fractal scaling we have observed. We also note that the same advection–dispersion equation that is used here (Eq. (8)) yields no fractal scaling (and thus is incompatible with the Plynlimon data) when it is used to model a single fixed-length flow path, with inputs at one end and outputs at the other (Kirchner et al., 2000). This implies that the fractal scaling exhibited by our simple model system (Fig. 3) depends on its spatially distributed character (although, as we show in Appendix A it does not require a particular geometric configuration). Thus, it appears that one must consider catchments as spatially distributed systems, but conventional distributed models require tuning large numbers of parameters, and thus are immune to rigorous testing (Beven and Binley, 1992; Kirchner et al., 1996). We are cautiously optimistic that approaches like the one presented here — spatially distributed, but not disaggregated into individually parameterized compartments — can provide a 'middle path' between box models and distributed models, contributing new insights into the hydrology and geochemistry of catchments.

Acknowledgements

Our collaboration was supported by the National Science Foundation through grants EAR-9357931, ATM-9628759 and EAR-9903281, and by the University of California. Sample collection and analysis were supported by the National Environment Research Council, the Environment Agency of England and Wales, and the Forestry Commission. We thank the Plynlimon field staff for sample collection, and M. Neal for sample analysis.

Appendix A. Effects of catchment geometry on tracer travel-time distributions and power spectra

In the analysis above, we assumed a particularly simple catchment geometry, in which the fraction of the contributing area at any given distance from the stream was a constant. Here, we explore how alternative catchment geometries affect the distribution of tracer travel times, and thus affect the power spectrum of tracer fluctuations.

The catchment travel-time distribution is determined by the constitutive equation for advective–dispersive transport (Eq. (8)), convolved with a weighting function $w(x)$ that describes the distribution of catchment area with distance x from the stream (see Eq. (9)). Since transport through the channel network is orders of magnitude faster than subsurface transport down hillslopes, it can be neglected for small

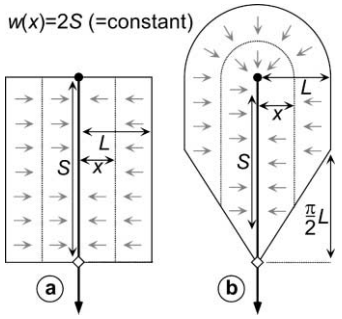

Fig. 7. Two catchment geometries that correspond to the weighting function, $w(x) =$ constant, used in Eqs. (10)–(12) and Figs. 4–6. The stream channel is denoted by the heavy line, the sampling point along it is denoted by the diamond symbol, and the channel head is denoted by the large dot. S is stream length, L is hillslope length, and the dashed line denotes all points a given distance x from the stream.

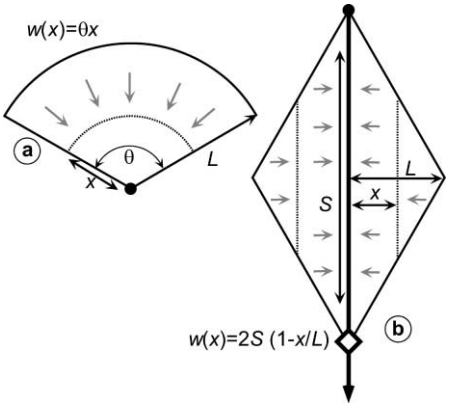

Fig. 8. Two end-member catchment geometries. One end-member case represents flow converging to a channel head from an amphitheater-shaped catchment: (a), such that the incremental drainage area represented by the weighting function $w(x)$ increases with distance from the channel. The other end-member case (b) represents a stream that reaches all the way to the head of a v-shaped valley, with a weighting function $w(x)$ that decreases with distance from the channel. Symbols are as in Fig. 7.

headwater catchments like ours. This implies that we need to concern ourselves only with the distribution of times (not the distribution of locations) at which a chemical tracer will reach the stream channel. Because transport through the channel network is fast enough to be considered instantaneous on the timescales of interest, the weighting function $w(x)$ is a complete description of the geometric factors controlling the catchment's travel-time distribution.

The weighting function used above to derive Eqs. (10)–(12), and thus to generate Figs. 4–6, is the simplest possible weighting function, $w(x) =$ constant. This weighting function obviously corresponds to the rather artificial catchment geometry shown in Fig. 7a, but it also characterizes the geometry shown in Fig. 7b, which is closer to the configuration of real-world catchments. Note that the configuration shown in Fig. 7b can include any stream length S, as long as $S \geq (\pi/2)L$. But although the weighting function $w(x) =$ constant is consistent with a not-too-unrealistic catchment configuration, it is unlikely to hold exactly in any real-world situation.

Spatially distributed advection and dispersion cannot be a plausible general model for fractal filtering in catchments, unless it generates that fractal filtering behavior for a suitably wide range of catchment geometries, not just for the idealized configuration shown in Fig. 7b. It is reasonable to expect that in some real-world catchments the incremental contributing area represented by $w(x)$ will increase with distance from the stream, while in other catchments it will decrease. We will therefore explore these two possibilities — $w(x)$ increasing, and decreasing, with distance from the stream — using two end-member catchment configurations and their associated weighting functions. We will then explore configurations that combine these two end-member cases in different proportions.

We first consider the case where the fractional contributing area $w(x)$ increases with distance from the stream. The end-member case, shown by Fig. 8a, corresponds to an amphitheater-shaped valley with subsurface flow converging to the channel head; tracer concentrations are measured at the channel head itself. In this configuration, the increment of contributing area $w(x)$ decreases with proximity to the channel head. One would expect, therefore, that the contribution of near-stream inputs (which are the source of the short-term responsiveness of the model system shown in Fig. 3) will be outweighed by inputs from upslope, which will have undergone more dispersion. One can test this conjecture mathematically by convolving the weighting function for this geometry ($w(x) = \theta x$, where θ is the angle over which flow converges to the channel head) with the advection–dispersion equation (Eq. (8)), and normalizing by the integral of the weights as described by Eq.

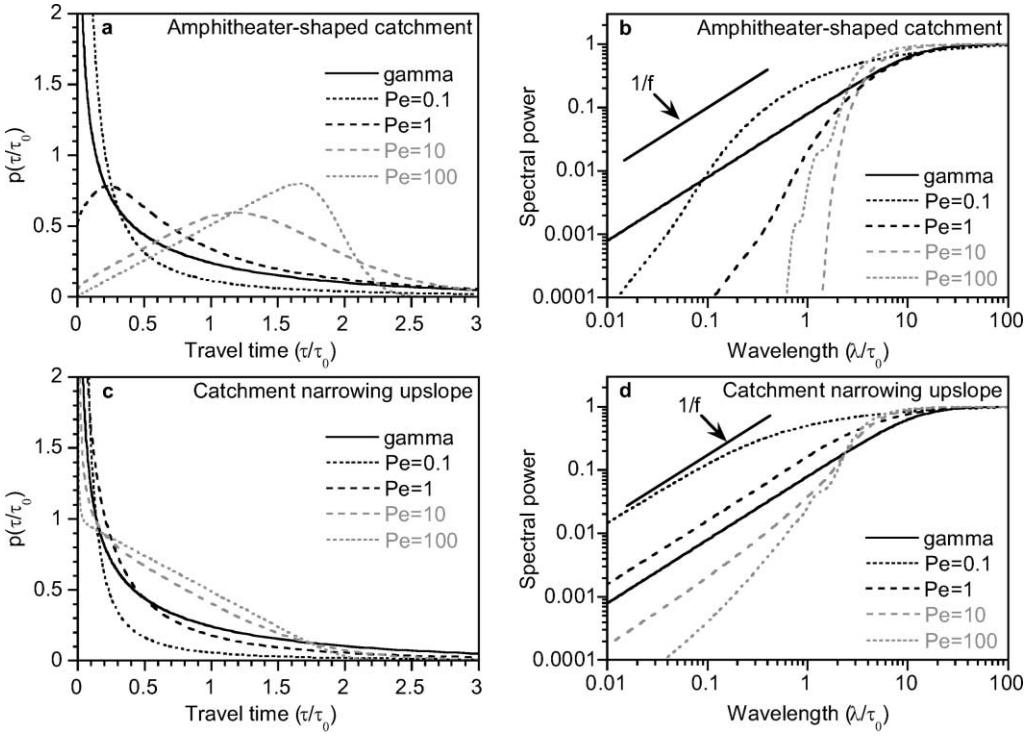

Fig. 9. Travel-time distributions and power spectra for the two end-member cases shown in Fig. 8. Convergent flow toward a channel head, as shown in Fig. 8a, yields travel-time distributions and power spectra that are inconsistent with the gamma distribution and $1/f$ scaling observed at Plynlimon (a,b). A catchment geometry in which the incremental contributing area $w(x)$ decreases upslope, as shown in Fig. 8b, yields travel-time distributions and power spectra that conform better to the observations at Plynlimon (c,d).

(9), yielding:

$$h(\tau) = \frac{2v}{L^2}\sqrt{\frac{D\tau}{\pi}}[e^{-(z_0)^2} - e^{-(z_L)^2}] - \frac{2}{L}\sqrt{\frac{D}{\pi\tau}}e^{-(z_L)^2} + \frac{1}{L^2}[2D + v^2\tau][\mathrm{erf}(z_L) - \mathrm{erf}(z_0)] \quad \text{(A1)}$$

where z_0 and z_L are expressed in dimensional form as

$$z_0 = -v\tau/\sqrt{4D\tau} \quad \text{and} \quad z_L = (L - v\tau)/\sqrt{4D\tau} \quad \text{(A2)}$$

Note that the travel-time distribution for this end-member case behaves differently from our simple one-dimensional model for parallel downslope flow (Eq. (10)). In the limit as τ approaches zero, this distribution does not approach infinity as $\tau^{-0.5}$, but instead approaches the finite value $2D/L^2$. Thus, this travel-time distribution lacks the short-term 'spike' seen in both the gamma distribution and in our simple model derived above. As before, we can non-dimensionalize the rate of dispersion using the Peclet number $Pe = vL/2D$, and we can non-dimensionalize the travel time as the dimensionless ratio $\tau/\tau_0 = \tau v/(L/2)$. With these substitutions, Eq. (A1) becomes a function only of the Peclet number and the dimensionless travel time τ/τ_0

$$h(\tau/\tau_0) = \frac{1}{Pe\sqrt{\pi}}[-z_0 e^{-(z_0)^2} - (z_L - 2z_0)\, e^{-(z_L)^2}] + \frac{1}{Pe}\left[\frac{1}{2} + z_0^2\right][\mathrm{erf}(z_L) - \mathrm{erf}(z_0)] \quad \text{(A3)}$$

where, as before, z_0 and z_L are expressed in

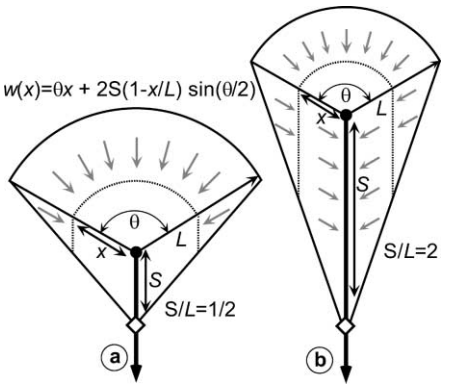

Fig. 10. Intermediate catchment geometries that combine the two end-member cases shown in Fig. 8. Both (a) and (b) are described by the same weighting function $w(x) = \theta x + 2S(1 - x/L)\sin(\theta/2)$, but they have different ratios of stream length S to hillslope length L, and therefore have different ratios of near-stream and upslope contributing areas. Symbols are as in Fig. 7.

non-dimensional form as

$$z_0 = -\frac{1}{2}\sqrt{Pe\tau/\tau_0} \qquad \text{and}$$
$$z_L = \sqrt{Pe/(\tau/\tau_0)} - \frac{1}{2}\sqrt{Pe\tau/\tau_0} \tag{A4}$$

The normalization constant $\tau_0 = L/2v$ is the time required for water to flow from the middle of the hillslope to the channel but, unlike in our simple one-dimensional model, τ_0 is no longer equal to the average travel time. The average travel time ($2L/3v$) is somewhat larger than τ_0, because there is more contributing area at the top of the hillslope than at the bottom.

Particularly for Peclet numbers near 1 or greater, the travel-time distribution for the end-member geometry shown in Fig. 8a does not resemble the gamma distribution (Fig. 9a). It is therefore not surprising that the power spectrum of this end-member travel-time distribution does not exhibit the $1/f$ scaling that is characteristic of our gamma distribution, and characteristic of the Plynlimon tracer data (Fig. 9b). In this end-member case, spatially distributed advection and dispersion yields a power spectrum with a log–log slope of 2 at Peclet numbers near 1 or less, and an even steeper slope at higher Peclet numbers.

Let us now consider the case where the fractional contributing area $w(x)$ decreases with distance from the stream channel. An end-member case, as shown in Fig. 8b, is a channel that flows down the entire length S of a v-shaped valley. The valley becomes wider downstream from the channel head, such that the catchment's incremental contributing area $w(x) = 2S(1 - x/L)$ decreases linearly from the stream channel to the divide. One would expect, therefore, that upslope inputs will have relatively little effect on the travel-time distribution, which instead will be dominated by near-stream inputs. As we have done above, we can derive the travel-time distribution by convolving our new weighting function with the advection–dispersion equation, and normalizing by the integral of the weights, yielding:

$$h(\tau) = \frac{2v}{L^2}\sqrt{\frac{D\tau}{\pi}}[e^{-(z_L)^2} - e^{-(z_0)^2}] + \frac{2}{L}\sqrt{\frac{D}{\pi\tau}}e^{-(z_0)^2} + \left[\frac{v}{L} - \frac{2D}{L^2} - \frac{v^2\tau}{L^2}\right][\mathrm{erf}(z_L) - \mathrm{erf}(z_0)] \tag{A5}$$

where the dimensional forms of z_0 and z_L are given by Eq. (A2). Note that in the limit as τ approaches zero, the first term of Eq. (A5) approaches infinity as $\tau^{-0.5}$ (just like our gamma distribution does), while the second term vanishes and the third term converges to $v/L - 2D/L^2$. Thus the short-term behavior of this distribution is similar to both our gamma distribution, and our simple one-dimensional model (Eq. (10)). Non-dimensionalizing as before, we derive the dimensionless form of Eq. (A5) as

$$h(\tau/\tau_0) = \frac{1}{Pe\sqrt{\pi}}[z_L\, e^{-(z_0)^2} - z_0\, e^{-(z_L)^2}] + \left[\frac{1}{2} - \frac{1}{Pe}\left[\frac{1}{2} + z_0^2\right]\right][\mathrm{erf}(z_L) - \mathrm{erf}(z_0)] \tag{A6}$$

where the dimensionless forms of z_0 and z_L are given by Eq. (A4). As above, the normalization constant $\tau_0 = L/2v$ is not quite equal to the average travel time, which is instead $L/3v$.

Except for Peclet numbers much greater than 1, this end-member geometry yields a travel-time distribution with short-term behavior similar to our gamma distribution (Fig. 9c). The power spectrum for this distribution exhibits $1/f$ scaling, except for Peclet

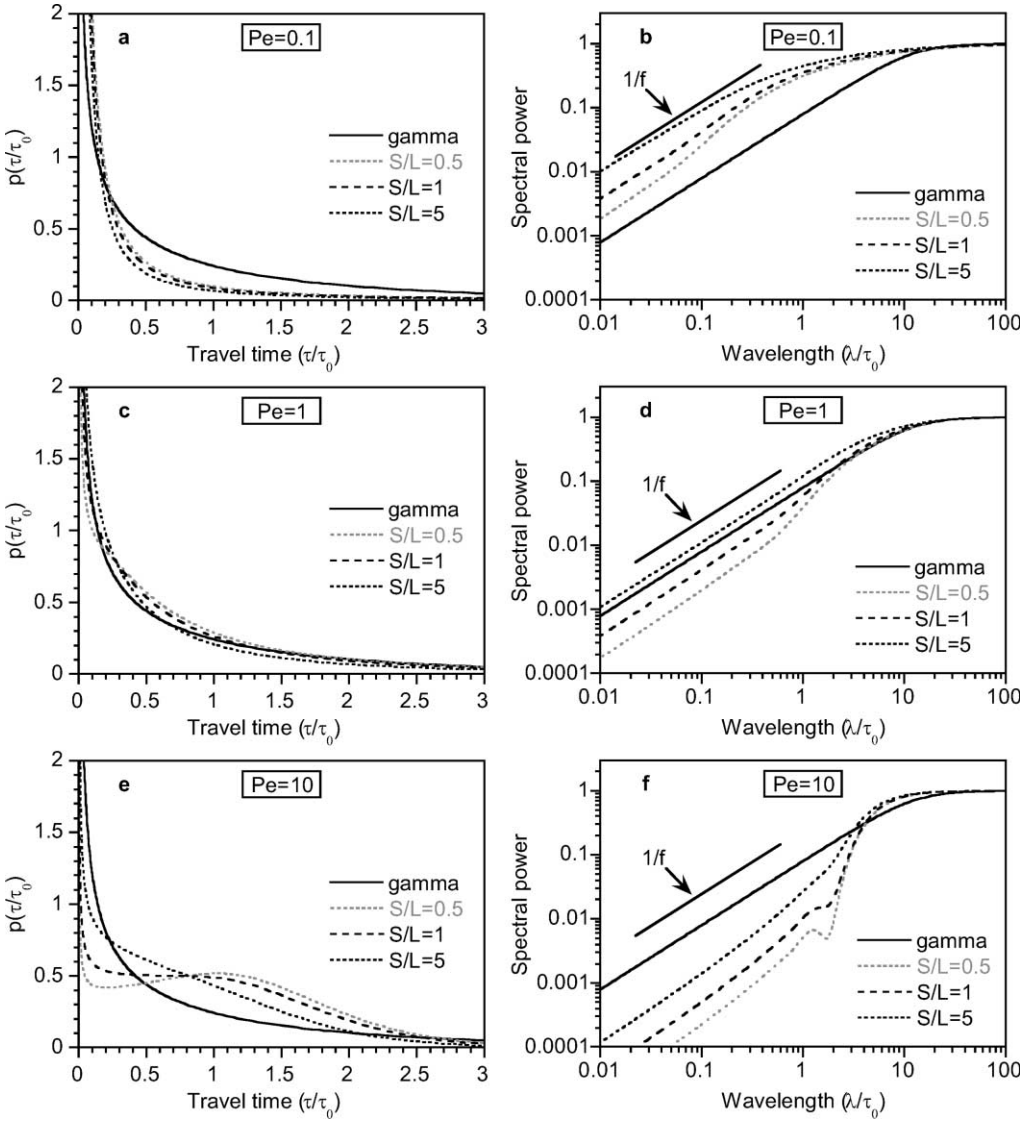

Fig. 11. Travel-time distributions and corresponding power spectra for intermediate catchment geometries (as shown in Fig. 10), characterized by three different ratios of stream length S to hillslope length L. Each panel compares three different catchment shapes under a single Peclet number; the gamma distribution is shown in each case for comparison. In each case, the weighting function is $w(x) = \theta x + 2S(1 - x/L)\sin(\theta/2)$ with $\theta = 2\pi/3 = 120°$, as shown in Fig. 10. For Peclet numbers near 1, spatially distributed advective–dispersive transport yields $1/f$ scaling, similar to that observed that Plynlimon, over a wide range of catchment shapes.

numbers much greater than 10 (Fig. 9d). Thus we see that spatially distributed advection and dispersion can generate fractal scaling similar to that seen at Plynlimon when the incremental contributing area decreases in the upslope direction (Figs. 8b and 9c–d), but not when it decreases to zero near the stream (Figs. 8a and 9a–b).

One of our end-member geometries (Fig. 8a) consistently violates the $1/f$ scaling seen at Plynlimon, while the other end-member case (Fig. 8b) consistently exhibits scaling near $1/f$, except at the largest Peclet numbers. Most real-world catchments will have configurations lying somewhere between our two end-member cases. Thus we need to determine

whether spatially distributed advection and dispersion will generate 1/*f* scaling over a wide range of geometries, or only in the end-member case. This question can be explored using catchment configurations that combine the two end-member cases in different proportions. Consider the class of configurations illustrated by the two examples in Fig. 10, which combine amphitheater-shaped valley heads (with flow converging to the channel head, as in Fig. 8a) and tapering valleys (with incremental contributing areas decreasing upslope, as in Fig. 8b). The weighting function that describes the class of configurations shown in Fig. 10 is $w(x) = \theta x + 2S(1 - x/L)\sin(\theta/2)$, with the ratio of stream length to hillslope length (S/L) controlling the relative proportions of near-stream and upslope contributing areas for any given valley head angle θ. The longer the valley relative to the hillslope length, and the farther the channel extends toward the divide, the smaller the proportion of the drainage area that will exhibit convergent flow like Fig. 8a, and the closer the catchment will conform to our second end-member case (as in Fig. 8b).

Performing the convolution in Eq. (9) using the weighting function in Fig. 10 directly yields the travel-time distribution for these intermediate catchment geometries:

$$h(\tau/\tau_0) = \frac{1}{Pe\sqrt{\pi}}[(w_2 z_L - w_1 z_0)\, e^{-(z_0)^2} - (w_1 z_L + (w_2 - 2w_1)z_0)\, e^{-(z_L)^2}] + \left[\frac{w_2}{2} + \frac{w_1 - w_2}{Pe}\left[\frac{1}{2} + z_0^2\right]\right][\mathrm{erf}(z_L) - \mathrm{erf}(z_0)] \quad \text{(A7)}$$

where z_0 and z_L are given in Eq. (A4), and w_1 and w_2 are

$$w_1 = \frac{(\theta/2)/\sin(\theta/2)}{(S/L) + (\theta/2)/\sin(\theta/2)} \quad \text{and} \quad w_2 = \frac{S/L}{(S/L) + (\theta/2)/\sin(\theta/2)} \quad \text{(A8)}$$

It can be seen that the travel-time distribution for these intermediate geometries (Eq. (A7)) is simply the weighted average of the travel-time distributions for the two end-member configurations (Eqs. (A3) and (A6)) with weights w_1 and w_2. In the case where S/L equals $(\theta/2)/sin(\theta/2)$, and thus the weights given to the two end-members are the same, the travel-time distribution becomes exactly equivalent to the simple one-dimensional model given in Eqs. (10) and (11).

For Peclet numbers near 1, these intermediate catchment configurations yield travel-time distributions that strongly resemble the gamma distribution, across a wide range of catchment shapes ($S/L \approx 0.5$ and greater; see Fig. 11c). Thus, at Peclet numbers near 1, many different catchment configurations yield 1/*f* scaling, similar to that observed at Plynlimon (Fig. 11d). Peclet numbers near 10 yield 1/*f* scaling in highly elongated catchments ($S/L \approx 5$), but in less elongated catchments one sees a 'step' in the power spectrum that is inconsistent with the Plynlimon data (see Fig. 11f). Peclet numbers near 0.1 yield approximate 1/*f* scaling across a wide range of catchment shapes (Fig. 11b), but, as seen in Table 2 above, they imply an implausibly long mean residence time of water in the catchment.

Here we have considered two end-member catchment geometries, and a range of intermediate configurations between them. This analysis yields three general results. First, advective–dispersive transport yields fractal 1/*f* scaling in a wide range of catchment configurations, as long as the Peclet number is near 1 or smaller. Second, the only catchment geometry in which advective–dispersive transport consistently fails to produce fractal 1/*f* scaling is a highly artificial one, in which the entire catchment runoff converges to a channel head, with no lateral stream inputs (Figs. 8a and 9b). Third, catchments require only small lengths of stream channel receiving lateral stream inputs (e.g. $S/L \approx 0.5$ in Figs. 10a and 11d) in order to generate 1/*f* scaling similar to that seen at Plynlimon. This leads to the conjecture that the short-wavelength fractal scaling seen at Plynlimon arises from advection and dispersion of near-stream inputs, with the shape and extent of the upslope portions of the catchment only controlling the convergence of the spectral power to its long-wavelength limit. Because nearly every catchment has near-stream zones in which rainfall inputs will advect and disperse, this conjecture implies that fractal 1/*f* scaling in tracer concentration time series, similar to that seen at Plynlimon, may be a nearly universal phenomenon characterizing a wide range of catchments.

References

Anderson, M.G., Burt, T.P., 1990. Subsurface runoff. In: Anderson, M.G., Burt, T.P. (Eds.). Process Studies in Hillslope Hydrology. Wiley, Chichester, pp. 365–400.

Anderson, S.P., Dietrich, W.E., Montgomery, D.R., Torres, R., Conrad, M.E., Loague, K., 1997. Subsurface flow paths in a steep, unchanneled catchment. Water Resources Research 33, 2637–2653.

Bain, L., 1983. Gamma distribution. In: Kotz, S., Johnson, N.L. (Eds.). Encyclopedia of Statistical Sciences. Wiley, New York, pp. 292–298.

Beven, K.J., Binley, A.M., 1992. The future of distributed models: model calibration and predictive uncertainty. Hydrological Processes 6, 279–298.

Bishop, K.H., 1991. Episodic increases in stream acidity, catchment flow pathways and hydrograph separation. PhD dissertation, University of Cambridge.

Bishop, K.H., Grip, H., O'Neill, A., 1990. The origins of acid runoff in a hillslope during storm events. Journal of Hydrology 116, 25–61.

Bracewell, R.N., 2000. The Fourier Transform and its Applications. 3rd ed. McGraw Hill, Boston.

Burns, D.A., Hooper, R.P, McDonnell, J.J., Freer, J.E., Kendall, C., Beven, K., 1998. Base cation concentrations in subsurface flow from a forested hillslope: the role of flushing frequency. Water Resources Research 34, 3535–3544.

Buttle, J.M., 1994. Isotope hydrograph separations and rapid delivery of pre-event water from drainage basins. Progress in Physical Geography 18, 16–41.

Chapman, P.J., Reynolds, B., Wheater, H.S., 1997. Sources and controls of calcium and magnesium in storm runoff: the role of groundwater and ion exchange reactions along water flowpaths. Hydrology and Earth System Sciences 1, 671–686.

Dershowitz, W., Miller, I., 1995. Dual-porosity fracture flow and transport. Geophysical Research Letters 22, 1441–1444.

Duffy, C.J., Gelhar, L.W., 1985. A frequency domain approach to water quality modeling in groundwater: theory. Water Resources Research 21, 1175–1184.

Duffy, C.J., Gelhar, L.W., 1986. A frequency domain analysis of groundwater quality fluctuations: interpretation of field data. Water Resources Research 22, 1115–1128.

Dunne, T., 1978. Field studies of hillslope flow processes. In: Kirkby, M.J. (Ed.). Hillslope Hydrology. Wiley, Chichester, pp. 227–294.

Gelhar, L.W., 1993. Stochastic Subsurface Hydrology. Prentice-Hall, Englewood Cliffs, NJ 390 pp.

Gelhar, L.W., Welty, C., Rehfeldt, K.R., 1992. A critical review of data on field-scale dispersion in aquifers. Water Resources Research 28, 1955–1974.

Gilman, K., Newson, M.D., 1980. Soil pipes and pipeflow — a hydrological study in upland Wales. Research Monograph No. 1. British Geomorphological Research Group, Norwich, pp. 1–110.

Hill, T., Neal, C., 1997. pH, alkalinity and conductivity in runoff and groundwater for the Upper River Severn catchment. Hydrology and Earth System Sciences 1, 697–715.

Kendall, C., Sklash, M.G., Bullen, T.D., 1995. Isotope tracers of water and solute sources in catchments. In: Trudgill, S.T. (Ed.). Solute Modeling in Catchment Systems. Wiley, New York, pp. 261–303.

Kirchner, J.W., Feng, X., Neal, C., 2000. Fractal stream chemistry and its implications for contaminant transport in catchments. Nature 403, 524–527.

Kirchner, J.W., Hooper, R.P., Kendall, C., Neal, C., Leavesley, G., 1996. Testing and validating environmental models. Science of the Total Environment 183, 33–47.

Kreft, A., Zuber, A., 1978. On the physical meaning of the dispersion equation and its solutions for different initial and boundary conditions. Chemical Engineering Science 33, 1471–1480.

Langmuir, D., 1997. Aqueous Environmental Geochemistry. Prentice-Hall, Saddle River, New Jersey 600 pp.

McDonnell, J.J., Stewart, M.K., Owens, I.F., 1991. Effect of catchment-scale subsurface mixing on stream isotopic response. Water Resources Research 27, 3065–3073.

Montgomery, D.R., Dietrich, W.E., Torres, R., Anderson, S.P., Heffner, J.T., Loague, K., 1997. Hydrologic response of a steep, unchanneled valley to natural and applied rainfall. Water Resources Research 33, 91–109.

Muscutt, A.D., 1990. Storm flow hydrochemistry of a small Welsh upland catchment. Journal of Hydrology 116, 239–249.

Neal, C., Kirchner, J.W., 2000. Sodium and chloride levels in rainfall, mist, streamwater and groundwater at the Plynlimon catchments, mid-Wales: inferences on hydrological and geochemical controls. Hydrology and Earth System Sciences 4, 295–310.

Neal, C., Rosier, P.T.W., 1990. Chemical studies of chloride and stable oxygen isotopes in 2 conifer afforested and moorland sites in the British uplands. Journal of Hydrology 115, 269–283.

Neal, C., Christophersen, N., Neale, R., Smith, C.J., Whitehead, P.G., Reynolds, B., 1988. Chloride in precipitation and streamwater for the upland catchment of the River Severn, mid-Wales: some consequences for hydrochemical models. Hydrological Processes 2, 155–165.

Neal, C., Wilkinson, J., Neal, M., Harrow, M., Wickham, H., Hill, L., Morfitt, C., 1997a. The hydrochemistry of the River Severn, Plynlimon. Hydrology and Earth System Sciences 1, 583–617.

Neal, C., Robson, A.J., Shand, P., Edmunds, W.M., Dixon, A.J., Buckley, D.K., Hill, S., Harrow, M., Neal, M., Wilkinson, J., Reynolds, B., 1997b. The occurrence of groundwater in the lower Palaeozoic rocks of upland Wales. Hydrology and Earth System Sciences 1, 3–18.

Neal, C., Hill, T., Alexander, S., Reynolds, B., Hill, S., Dixon, A.J., Harrow, M., Neal, M., Smith, C.J., 1997c. Stream water quality in acid sensitive UK upland areas, an example of potential water quality remediation based on groundwater manipulation. Hydrology and Earth System Sciences 1, 185–196.

Neal, C., Hill, T., Hill, S., Reynolds, B, 1997d. Acid neutralization capacity measurements in surface and ground waters in the Upper River Severn, Plynlimon: from hydrograph splitting to water flow pathways. Hydrology and Earth System Sciences 1, 687–696.

Neuman, S.P., 1990. Universal scaling of hydraulic conductivities and dispersivities in geologic media. Water Resources Research 26, 1749–1758.

Niemi, A.J., 1977. Residence time distributions of variable flow processes. International Journal of Applied Radiation and Isotopes 28, 855–860.

Nyberg, L., Rodhe, A., Bishop, K., 1999. Water transit times and flowpaths from two line injections of ^{3}H and ^{36}Cl in a micro-catchment at Gardsjon, Sweden. Hydrological Processes 13, 1557–1575.

Robson, A., Neal, C., Hill, S., Smith, C.J., 1993. Linking variations in short-term and medium-term stream chemistry to rainfall inputs — some observations at Plynlimon, mid-Wales. Journal of Hydrology 144, 291–310.

Rodhe, A., Nyberg, L., Bishop, K., 1996. Transit times for water in a small till catchment from a step shift in the oxygen-18 content of the water input. Water Resources Research 32, 3497–3511.

Scargle, J.D., 1982. Studies in astronomical time series analysis. II. Statistical aspects of spectral analysis of unevenly spaced data. The Astrophysical Journal 263, 835–853.

Schnoor, J.L., 1996. Environmental Modeling: Fate and Transport of Pollutants in Water, Air, and Soil. Wiley, New York 682 pp.

Sklash, M.G., 1990. Environmental isotope studies of storm and snowmelt runoff generation. In: Anderson, M.G., Burt, T.P. (Eds.). Process Studies in Hillslope Hydrology. Wiley, Chichester, pp. 401–435.

Sklash, M.G., Beven, K.J., Gilman, K., Darling, W.G., 1996. Isotope studies of pipeflow at Plynlimon, Wales, UK. Hydrological Processes 10, 921–944.

Soulsby, C., Chen, M., Ferrier, R.C., Helliwell, R.C., Jenkins, A., Harriman, R., 1998. Hydrogeochemistry of shallow groundwater in an upland Scottish catchment. Hydrological Processes 12, 1111–1127.

Soulsby, C., Malcolm, R., Helliwell, R., Ferrier, R.C., Jenkins, A., 2000. Isotope hydrology of the Allt a' Mharcaidh catchment, Cairngorms, Scotland: implications for hydrological pathways and residence times. Hydrological Processes 14, 747–762.

Sposito, G., White, R.E., Darrah, P.R., Jury, W.A., 1986. A transfer function model of solute transport through soil 3. The convection–dispersion equation. Water Resources Research 22, 255–262.

Toth, J., 1963. A theoretical analysis of groundwater flow in small drainage basins. Journal of Geophysical Research 68, 4795–4812.

Tsang, C.F., Neretnieks, I., 1998. Flow channeling in heterogeneous fractured rocks. Reviews of Geophysics 36, 275–298.